Simulation Study on the Diffusive Motion in Deeply Supercooled Water

Dietmar Paschek and Alfons Geiger*

Physikalische Chemie, Universität Dortmund, 44221 Dortmund, Germany

Received: October 14, 1998; In Final Form: February 25, 1999

The diffusion process in supercooled liquid water has been studied by a series of molecular dynamics simulations using systems of 216 ST2-model molecules in the temperature range between 255 and 360 K. In contrast to SPC/E water (*Phys. Rev. E* **1996**, *54*, 6331), the ST2 liquid does *not* show the appearance of a kinetic glass transition with structural arrest. Instead, we observe a significant change of the diffusion mechanism in the deeply supercooled region. The high-temperature microstep diffusion mechanism transforms continuously into a jump-diffusive behavior at low temperatures. By analyzing the intermediate incoherent structure factor of the center of mass motion we can characterize the hopping process by an average residence time τ_0. The hopping process is found to control reorientational and translational motions, leading to a second region of apparent Arrhenius behavior with a high activation energy of about 115 kJ mol^{-1}. The change in the dynamic behavior occurs in parallel to the structural and thermodynamical transformation to a low-density liquid form of ST2 water.

1. Introduction

In supercooled water, an apparent divergence of various thermodynamic and dynamic properties has been observed.[1] Essentially, three different explanations for this behavior have been discussed.

The stability limit conjecture[2−5] suggests that the strong variation in the *thermodynamic* properties is caused by the existence of a spinodal line which proceeds continuously from the supercooled state to the gas−liquid critical point. A more recent approach, deduced from an extensive series of molecular dynamics (MD) simulations[6−10] identifies as the origin of the increasing fluctuations the existence of a second critical point in the metastability region, which terminates the coexistence line of two distinct states of supercooled water. Several other theoretical studies also support the idea of a metastable critical point.[11−13] At even lower temperatures, the two liquid phases eventually turn into two coexisting phases of amorphous ice. Both scenarios, the spinodal line as well as the metastable critical point, can be reproduced by incorporating the effect of hydrogen bonding into a van der Waals type equation of state.[14]

A singularity-free explanation of the experimentally observed anomalies in supercooled water is furnished by the percolation or 'transient gel' model[15,16] and the lattice fluid model.[17] Both predict a nondiverging but strong increase of the response functions. Experimental evidence for the existence of a liquid−liquid phase transition has been proposed lately by Mishima and Stanley,[18] but due to the experimental difficulties, none of the mentioned scenarios has so far been proved or disproved unambiguously.

Recently, it has been suggested by Sciortino and co-workers[19−21] to interpret the apparent divergence of *dynamic* properties at the so-called Angell temperature[22,23] as being due to a kinetic glass transition, as predicted by the idealized mode coupling theory.[24] These conclusions are based on molecular dynamics simulations using the SPC/E model,[25] which reveals the occurrence of a complete structural arrest at approximately 200 K at $P = -80$ MPa (and 186 K at atmospheric pressure).

In this contribution, we report the results of a MD simulation study using the ST2 model potential.[26] From various simulation studies it is well-known that the SPC/E and ST2 potentials "bracket" real water in the sense that ST2 overestimates the structuredness and the anomalous properties of real water, while SPC/E underestimates them.[27] For example, in the SPC/E study of Sciortino et al.,[20] the density maximum is located at 240 K, while in the study presented here, the density maximum is at 310 K.

In this paper, we focus on the single particle dynamics and suggest a change in the underlying diffusion mechanism as the origin of the observed strong variation of the apparent activation energy of the dynamic properties. A transition from microstep diffusion to jump diffusion comparable to the one observed here has been observed, for example, in molecular dynamics simulation studies of a density-induced glass transition in simple Lennard-Jones fluids.[28] However, in this diffusivity range, far from a glass transition point, such a changeover has not been seen before, to our knowledge.

Jump diffusion is a frequently and controversially discussed feature of the molecular dynamics of water.[29−34] There is evidence from quasielastic incoherent neutron scattering, showing a deviation of the measured line broadening from the ideal Dq^2 behavior even at room temperature.[29] Extensive quasielastic neutron scattering experiments, extended to the supercooled region,[30,31] forced the conclusion that jump diffusion is prevailing at low temperatures. Teixera et al.[31] found that their experimental data could be fitted well to a model dividing the intermediate scattering function into a vibrational part, represented by a Debye−Waller factor, a rotational part based on the Debye model for spherical top rotational diffusion, and a translational part using a Singwi−Sjölander[35,36] type jump-diffusion concept. The most important feature of their analysis, the jump-diffusive behavior, becomes evident in the supercooled regime with the half width at half-maximum (HWHM) of the scattering function asymptotically approaching a constant value

TABLE 1: Parameters Characterizing the Performed MD-Simulations

T/K	p/MPa	$\rho/g\ cm^{-3}$	$E_{pot}/kJ\ mol^{-1}$	N_{nn}	t_d/ps	t_t/ps
255	99.6	0.883	−48.12	4.107	14400	17000
260	111.0	0.894	−47.30	4.186	844	1696
265	81.4	0.910	−46.19	4.290	640	1440
270	84.3	0.942	−44.97	4.471	400	1000
275	77.8	0.957	−44.16	4.574	400	1000
280[b]	80.3	0.967	−43.65	4.643	240	500
290	80.9	0.986	−42.59	4.756	300	900
300[b]	80.4	0.994	−41.73	4.824	120	240
330[b]	82.4	0.994	−39.61	4.851	120	240
360[b]	73.8	0.978	−37.59	4.768	120	240

[a] The averages of the pressure, p, density, ρ, and potential energy, E_{pot} correspond to the total simulation. The number of nearest neighbors N_{nn} was obtained by integrating the O−O pair correlation function to the position of the first minimum. t_d is the length of the last part of the simulation which was analyzed with respect to the molecular dynamics. t_t denotes the total simulation length. [b] Indicates simulations with a time step of 1 fs. The default time step is 2 fs.

of $1/\tau_0$ at increased q.[31] The mean residence time τ_0 is accordingly found to vary strongly with the temperature.

On the other hand, Rahman and Stillinger in their famous contribution[37] classified such an interpretation as definitively conflicting with their simulation results for a temperature of 310 K. Moreover, in a recent MD study on supercooled SPC/E water, Chen et al.[34] qualify the jump-diffusion picture. According to their findings, the observed HWHM behavior of $S(q,\omega)$ can be attributed to a Kohlrausch-like incoherent intermediate structure factor with a q-dependent stretched exponential, β, revealing a "saturation" behavior of the HWHM, like the one observed experimentally. But, in this context, the obtained $1/\tau_0$ would not have physical meaning. Unfortunately, the experimental resolution in ref 31 did not allow a more detailed line-shape analysis to confirm a Kohlrausch behavior for real water.

2. MD Simulations

We present a molecular dynamics study on supercooled liquid water, using a system of 216 ST2-model[26] molecules. The Rahman−Stillinger ST2 potential is employed, because it reproduces the anomalous properties of real water well and reveals a density maximum at a higher temperature compared to real water.[6] As mentioned in the Introduction, other common effective pair potentials such as TIP4P[38] and SPC/E[25] are found to exhibit a density maximum shifted to much lower temperatures.[7,39] Taking into account the reduced molecular mobility in the supercooled state as well as the limited time range accessible to MD simulations, the ST2 potential seems to be well suited for a study of the dynamic properties beyond the density maximum. In consideration of the phase diagram shift between real water and ST2-model water, we study the 80 MPa isobar which is known to exhibit a density maximum of 1.0 g cm^{-3} at a temperature of 310 K.[6] In the range between 255 and 360 K, 10 simulation runs were performed (Table 1). We employed a standard leap-frog/SHAKE MD scheme[40] with time steps given in Table 1. The forces were truncated at cut-off distances of half the box-length. Cut-off corrections were considered by usage of a Steinhauser reaction-field term[41] in combination with Lennard-Jones corrections for virial and potential energy. Constant-temperature conditions were achieved by applying the Berendsen weak coupling procedure[42] ($\tau_T =$ 0.5 ps). The chosen densities were determined by preliminary trial runs and are in perfect agreement with the data reported in ref 7. The effect of different time step lengths (1 and 2 fs) on dynamical and thermodynamical properties has also been
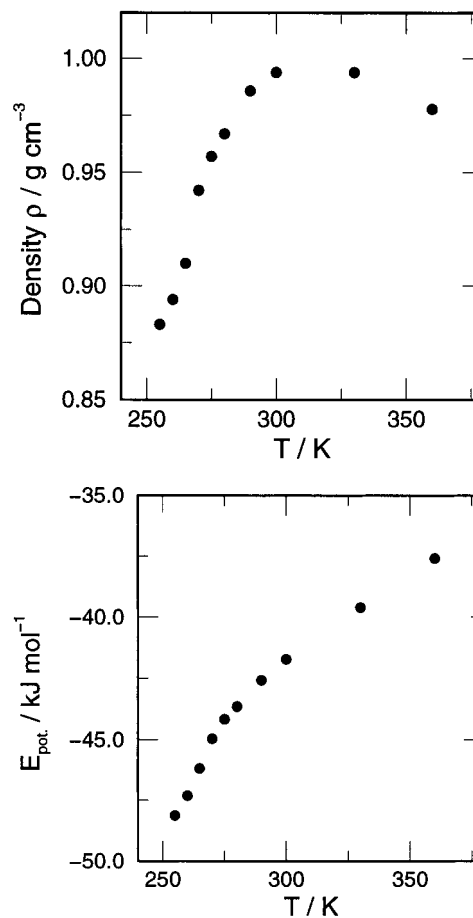

Figure 1. Temperature dependence of the density ρ and potential energy E_{pot} of ST2 water along the 80 MPa isobar.

checked for various temperatures and was found to be negligible. Due to the position of the line of density maxima in the $p−T$ phase diagram[6,7] as well as the position of the melting line of ST2 water,[43] the considered temperature interval corresponds to a range extending to about 220 K in real water, well below experimentally accessible temperatures.

3. Thermodynamic and Structural Properties

In Figure 1 thermodynamic properties along the considered isobar are depicted. The temperature dependence of the mass density and potential energy allows us to discuss further the location of the studied isobar with respect to the phase diagram of other waterlike models. In accord with the phase diagram proposed by Poole et al.[14] and the volumetric behavior of the lattice model of Rebelo et al.,[17] we denote the existence of a region of positive curvature of $\rho(T)$ when entering the low-temperature regime. This indicates that at the lowest temperatures the ST2 liquid has passed a sharp change to a low-density liquid form. The potential energy shows a significantly increased temperature dependence below 270 K. It can be inferred from the data that C_p exhibits a maximum in the interval between 260 and 270 K. Again, this behavior could be produced either by passing the second critical point of the two-liquid scenario[14] or from abrupt but continuous changes, as observed in the singularity free model.[17]

Note the differences from the observations made for super-cooled SPC/E water in the study of Sciortino et al.[20] The strong increase in the temperature dependence of E_{pot} as well as the mentioned density behavior is not observed in their study. These
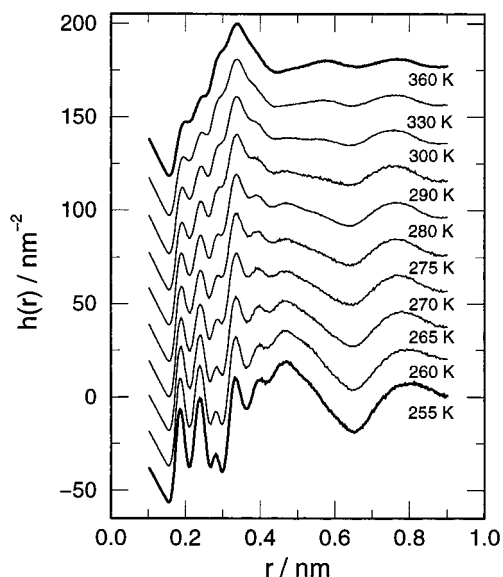
Figure 2. Composite radial distribution function $h(r)$ (eq 1), indicating an approach to the low-density amorphous ice structure at low temperatures (compare with experimental curves in refs 45−47).

differences are in agreement with MD simulations on the phase diagram of SPC/E water and can be explained by the phase diagram shift between ST2 and SPC/E water.[27] This gives further support to speak of *deeply supercooled* water with respect to the ST2 phase diagram.

In parallel with the changes in the thermodynamic properties, Figure 2 shows the structural changes in the examined temperature range. Given are the composite radial distribution functions[44]

$$h(r) = 4\pi\left(\frac{N}{V}\right)r[0.092g_{OO}(r) + 0.486g_{HH}(r) + 0.422g_{OH}(r) - 1] \quad (1)$$

to compare with the results of neutron scattering experiments on D_2O. With decreasing temperature $h(r)$ approaches in a striking way the experimental low-density amorphous ice (LDA) structure. (For comparison see refs 45 and 46.) The high-temperature radial distribution function more closely resembles the high-density amorphous ice (HDA) form.[45,47]

Figure 3 illustrates the differences between the high- and low-temperature structures. It shows the probability distribution of the so-called "tretrahedricity measure"[48]

$$M_T = \frac{\sum_{i>j}(l_i - l_j)^2}{15\langle l^2\rangle} \quad (2)$$

where l_i are the lengths of the six edges of the tetrahedron formed by the four nearest neighbors of a given water molecule. For an ideal tetrahedron, M_T is zero. M_T increases with increasing distortion. From Figure 3 we can see that at 255 K we have only very few strongly distorted nearest neighbor surroundings, whereas at 360 K these local structures prevail. At intermediate temperatures, a bimodal distribution is indicated. This suggests distinguishing two kinds of local structures, one more LDA-like and the other more HDA-like, and that both structures coexist with varying ratio. Recent neutron diffraction studies on the structure of supercooled water support such a picture.[49]
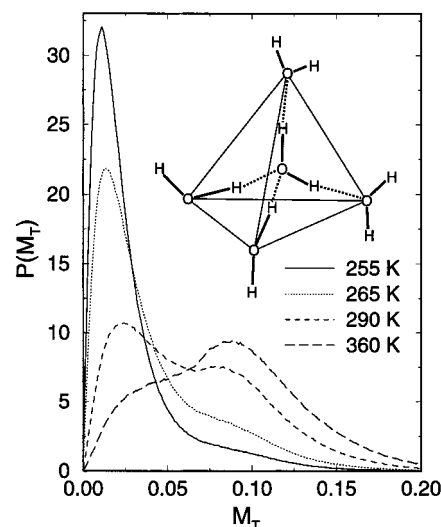

Figure 3. Distribution of the tetrahedricity measure M_T (eq 2), suggesting a temperature-dependent coexistence of two distinguishable types of local water structures.
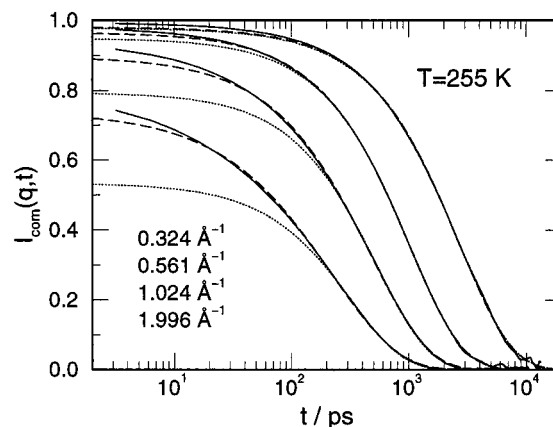

Figure 4. Intermediate incoherent structure $I_{com}(q,t)$ of the center of mass motion at 255 K for four different q values (solid lines). The dotted and dashed lines represent fits according to eq 4. For the dotted curves $I_{com}(q,t)$ has been considered only for times longer than 200 ps, whereas for the dashed curves the complete data set has been used. As shown in Figure 5, the long-time behavior turns out to become exponential.

Finally, we should note that our simulation series enters the temperature region where the conversion to a low-density LDA-like structured liquid has almost been completed.

4. Dynamics in the Deeply Supercooled Range

4.1. Center of Mass Motion. From the trajectory data we calculate the intermediate incoherent structure factor for the center of mass (com) motion $I_{com}(q,t)$ explicitly.

$$I_{com}(q,t) = \langle\langle e^{-i\vec{q}\,\vec{r}_{com}(0)} e^{+i\vec{q}\,\vec{r}_{com}(t)}\rangle\rangle_q \quad (3)$$

Averaging is performed over four different momentum-transfer vectors $\vec{q}$ for each depicted q value. The time-correlation functions were calculated applying a fast Fourier transform procedure[50] using approximately 1.6×10^4 stored configurations per run extending over the time range t_d given in Table 1. The $I_{com}(q,t)$ for different q values for $T = 255$ K are shown in Figure 4. We consider the experimentally probed q range between 0.3 and 2.0 Å^{-1} [31] and determine $I_{com}(q,t)$ for 17 different momentum transfers, q, at each temperature.
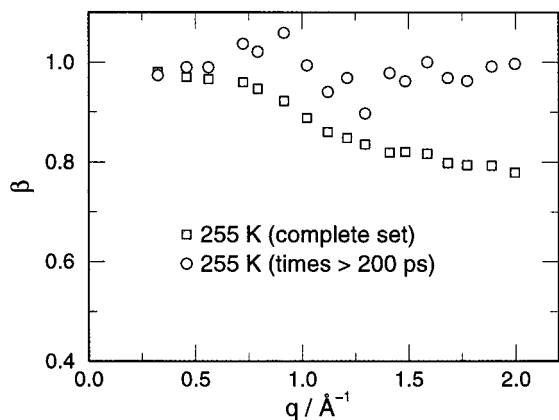
Figure 5. Stretching exponent β obtained from fits of $I_{com}(q,t)$ to eq 4. When considering the long-time behavior ($t > 200$ ps), no systematic deviation of β from 1 can be noted.

As indicated in Figure 4, the obtained correlation functions may be generally expressed in terms of a Kohlrausch law showing a stretched exponential behavior according to

$$I_{com}(q,t) = A(q) \exp\left[-\left(\frac{t}{\tau_q}\right)^\beta\right] \qquad (4)$$

In view of the fact that Sciortino et al.[19,20] discuss a stretched exponential decay of $I_{com}(q,t)$ with β revealing a strong q dependence, we consider the validity of a corresponding description here. We have to denote that, while considering the complete time range, our fit systematically obtains exponents β smaller than 1 at increasing q (as outlined in Figure 5). This effect is attributed to the presence of a "cage motion" in the intermediate time range. Instead, when considering the long-time behavior (i.e., $t > 200$ ps for 255 K), an exponential behavior with $\beta = 1$ is recovered again (see also Figure 5). So, for the observed q range and times larger than τ_0 (given below), we generally do not find a significant deviation of the stretching exponent β from 1.

For the limit of $\beta \to 1$, the inverse relaxation time τ_q^{-1} corresponds to the HWHM of a Lorentzian-shaped incoherent dynamic structure factor $S_{com}(q,\omega)$. Thus, we apply eq 4 (with $\beta = 1$) to derive τ_q from the long time slope of $I_{com}(q,t)$. For jump diffusion with an exponential distribution of jump lengths, the HWHM of $S(q,\omega)$ is determined by[35,36]

$$\tau_q^{-1} = \frac{Dq^2}{1 + Dq^2\tau_0} \qquad (5)$$

where D is the self-diffusion coefficient and τ_0 can be identified with the mean residence time of the diffusing particle between two jumps. The residence times τ_0 were obtained as the slope of a plot of $\tau_q\, q^2$ vs q^2 and are given in Table 2. The self-diffusion coefficients D obtained from the intersection are in good agreement with values taken from the mean square displacement of the molecules, applying the Einstein relation

$$D = \frac{1}{6}\lim_{\tau\to\infty}\frac{\partial}{\partial\tau}\langle[\vec{r}_{com}(0) - \vec{r}_{com}(\tau)]^2\rangle \qquad (6)$$

At higher temperatures than 275 K, τ_q^{-1} exhibits a nearly linear q^2 dependence, so the τ_0 would become too small to be compatible with a reasonable definition of a *residence time*. This also indicates that with incrasing temperature the jump-diffusion model becomes less appropriate. The extracted average jump lengths $l_0 = (6D\tau_0)^{1/2}$ (Table 2) are found to be between 1.3

TABLE 2: Translational Diffusion Constants, D, Mean Residence Times, τ_0, and Reorientational Correlation Times, τ_2, Obtained from the Simulation Runs[a]

T/K	$D/10^{-9}$ m^2 s^{-1}	τ_0/ps	l_0/Å	τ_2(OH)/ps	τ_2(O)/ps
255	4.1×10^{-2}	270	2.6	220	220
260	1.1×10^{-1}	70	2.2	81	79
265	2.8×10^{-1}	17	1.7	23	25
270	6.3×10^{-1}	4.7	1.3	11	10.4
275	9.8×10^{-1}	3.0	1.3	6.1	5.3
280	1.3			4.1	3.9
290	1.9			2.5	2.3
300	2.4			1.7	1.6
330	4.4			0.9	0.8
360	6.8			0.54	0.46

[a] τ_2(OH) represents the correlation of the O–H bond vector, while τ_2(O) describes the reorientation of the O normal to the molecular plane vector. l_0 is the average "jump length".
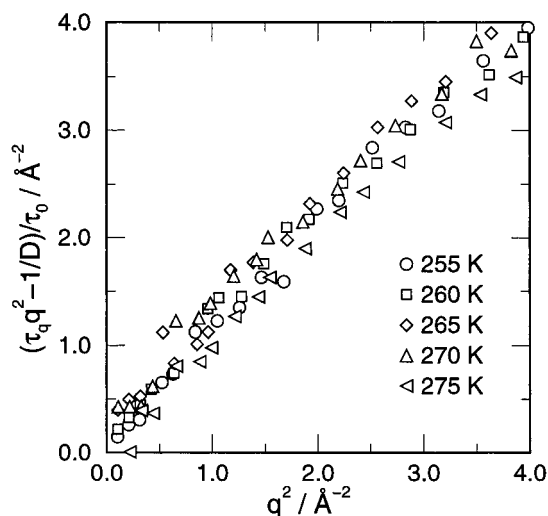

Figure 6. Scaled plot of the inverse half width at half-maximum (HWHM) τ_q of the quasielastic incoherent scattering function for the center of mass motion for different temperatures vs q^2. A strict validity of eq 5 should reveal a slope of 1. The diffusion coefficients D were obtained independently from the center of mass mean square displacements, whereas the average residence times τ_0 were obtained from plots of $\tau_q q^2$ vs q^2.

and 2.6 Å in the observed temperature range with a tendency to increase with decreasing temperature. The highest temperature data match roughly the value of 1.23 Å experimentally obtained by Chen et al.[30] for real water, whereas the temperature dependence of l_0 is in accordance with the tendency observed by Teixeira et al.[31]

To check the appropriateness of this approach, we present in Figure 6 a plot of $(\tau_q q^2 - D^{-1})\tau_0^{-1}$ vs q^2 according to eq 5. As can be seen, this leads to a rather consistent description of the data in the temperature range below 280 K. In Figure 6, the independently obtained D values (from eq 6) were used.

At this stage, we can conclude that the behavior of the quasielastic line broadening is consistent with a jump-like relaxation in the deeply supercooled ST2 liquid. The observed phenomenon is strictly attributed to the center of mass motion of the molecules. Since we focus on the long-time relaxation process, we have to emphasize that our approach does not provide a *complete* description of the center of mass motion. A further detailed treatment, including the short and intermediate time-range remains necessary.

To record jump diffusion more directly, we calculate the van Hove self-correlation function[51] for the center of mass motion, displayed for two temperatures in parts a and b of Figure 7. $G_{self}(r,t)$ denotes the probability of finding a particle
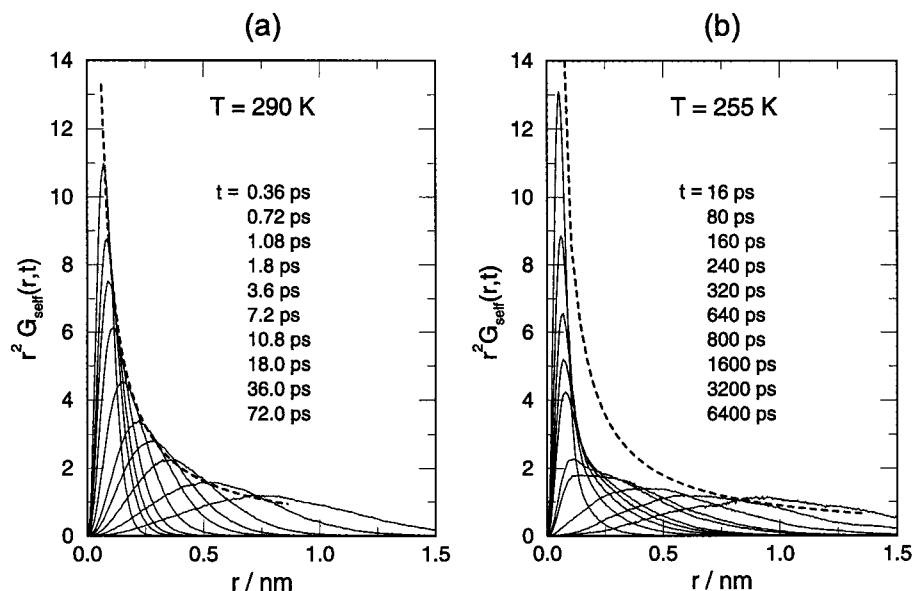
Diffusive Motion in Deeply Supercooled Water

J. Phys. Chem. B, Vol. 103, No. 20, 1999 **4143**

Figure 7. Van Hove self-correlation functions $G_{self}(r,t)$ for the center of mass motion of water molecules at two different temperatures: (a) 290 K; (b) 255 K. The broken curve is the line of maxima of perfect Gaussian distributions (eq 7) for varying times t and diffusion coefficients $D = 1.9 \times 10^{-9}$ m^2 s^{-1} (290 K) and $D = 4.1 \times 10^{-11}$ m^2 s^{-1} (255 K).]

at a certain distance r from the location where it resided at time $t = 0$.

Figure 7 reveals a qualitative change in the diffusion behavior with decreasing temperature. At 290 K (Figure 7a) we find at any diffusion time a unimodal Gaussian distribution with a strongly shifting maximum position, as expected for continuous microstep diffusion. At the lower temperature (Figure 7b) and intermediate diffusion times, we observe the appearance of a pronounced shoulder, whereas the position of the first peak remains nearly constant. For long times, the first maximum vanishes and the second peak starts to evolve to a purely Gaussian shape again. To monitor deviations from Gaussian behavior, the broken lines indicate in parts a and b of Figure 7 the positions of the maxima in case of a pure Gaussian form

$$r^2 G_{self}(r,t) = r^2 (4\pi Dt)^{-3/2} \exp\left(-\frac{r^2}{4Dt}\right) \qquad (7)$$

with diffusion coefficients $D = 4.1 \times 10^{-11}$ m^2 s^{-1} and $D = 1.9 \times 10^{-9}$ m^2 s^{-1} taken from the mean square displacements at 255 and 290 K, respectively. We see that for intermediate times at the low temperature the maximum position lags behind the Gaussian, indicating arrest between jumps. At longer times, when averaging over many jumps occurs, Gaussian behavior is recovered again.

The occurrence of a broad shoulder rather than a second peak at intermediate times demonstrates a broad distribution of jump lengths. This is in agreement with the Singwi–Sjölander model[36] which has been used to describe the q dependence of the incoherent dynamic structure factor.

A direct look at the molecular trajectories supports the jump diffusion picture. In Figure 8, the trajectory of a single molecule taken from the 260 K run is depicted. The location of the oxygen atom is displayed by a closed line, while the positions of the hydrogen atoms are represented by dots. A run of 844 ps length is shown. The jumplike motion becomes evident by revealing several clearly distinguishable regions of residence. The size of the depicted cube is 1 nm, so it has to be noted that some of the jumps extend to several angstroms. There is certainly a cooperative rearrangement of the surrounding hydrogen bond network necessary to enable molecules to perform such long
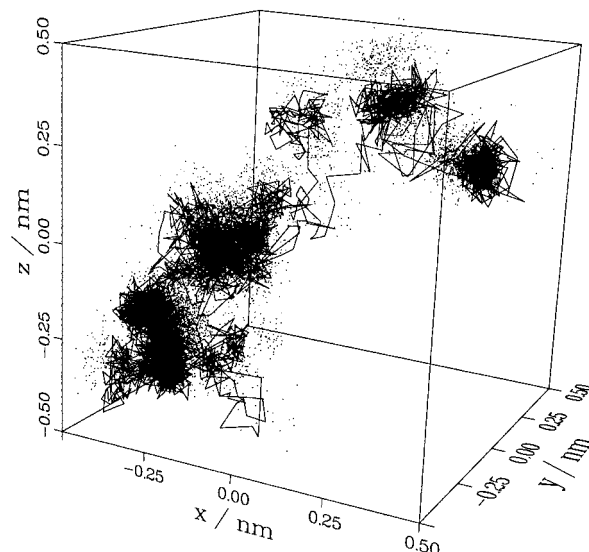

Figure 8. Trajectory of a single molecule taken from the 260 K simulation run. The closed line represents the oxygen path. The hydrogen positions are represented by dots.

jumps. It was observed that an increased concentration of hydrogen bonding possibilities promotes the restructuring of the hydrogen bond network.[52–54] The jump process may thus be correlated to fluctuations in the surrounding local density of hydrogen bond donor or acceptor sites. This becomes evident from monitoring the number of nearest neighbors of a jumping particle. In Figure 9 such an event taken from the lowest temperature run is depicted. It strongly suggests that the jumps are correlated to the appearance of a fifth neighbor in the vicinity of the jumping particle.

By looking at trajectories at intermediate temperatures, we find that both types of motion, microstep diffusion (identified by continuous trajectories without well separated regions of residence) and jump diffusion occur simultaneously. This suggests that a pure microstep diffusion at temperatures above 280 K is continuously transforming into a prevailing jump diffusion at 255 K by the coexistence of differently structured regions of changing fraction. Evidence for the validity of such
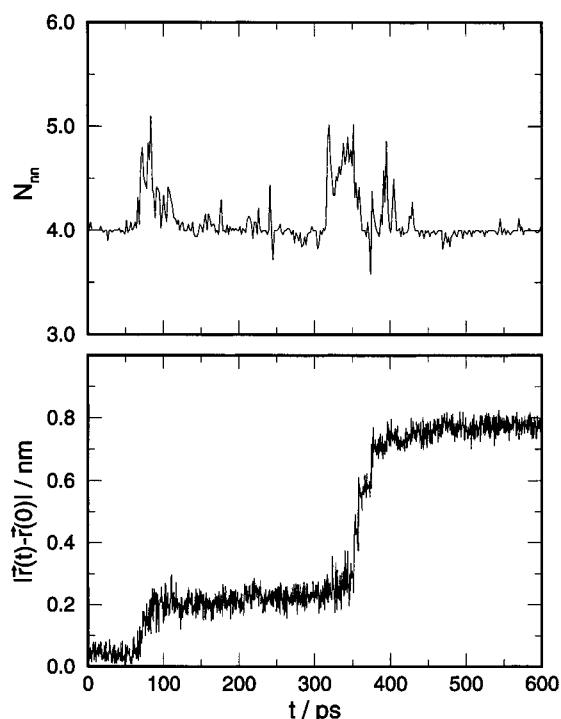
4144 *J. Phys. Chem. B, Vol. 103, No. 20, 1999*

Paschek and Geiger

Figure 9. Change of the local environment of a jumping particle suggesting that the appearance of a fifth neighbor and the occurrence of the jumps are correlated: (a) number of nearest neighbors of a selected molecule as a function of time; (b) displacement of the center of mass of the same molecule.

a structural behavior comes from a recent neutron diffraction study of Bellissent–Funel.[49] Further evidence from MD simulations we will present in a subsequent paper.

4.2. Jump Diffusion and Temperature Dependence of Reorientational and Translational Motions. To show how the observed jump mechanism affects both the translational and the reorientational motion, we additionally calculate the reorientational correlation times for two molecular vectors. Namely, the O–H bond and the O normal to the molecular plane vector. The correlation times τ_2 are obtained by integrating correlation functions of the form

$$C_2(t) = \frac{\langle P_2[\theta(0)]P_2[\theta(t)]\rangle}{\langle P_2[\theta(0)]^2\rangle} \tag{8}$$

$P_2[\theta]$ is the second Lengendre polynomial of the angle between a certain molecule fixed vector and the z axis of the system frame. The obtained correlation times are linearly related to the ^{17}O NMR (O normal to the molecular plane) and ^{2}H NMR (O–H) relaxation rates.[55,56]

First, we can denote that both vectors exhibit the same correlation times over the whole temperature range (see Table 2). The molecular reorientation seems to be isotropic. In Figure 10 the temperature dependence of the reorientational correlation times and the self-diffusion coefficients for ST2 water are compared with experimental values.[22,23,57–60] The dashed curves represent analytic power law expressions obtained from fits to experimental values.[22,23,59,61]

Whereas the agreement between the dynamic properties of real water and ST2 water in the ambient temperature range is astonishing but not unexpected (after all ST2 has been furnished to reproduce well the properties at ambient temperature), there are pronounced deviations at lower temperatures. Both dynamic properties of ST2 water change their temperature dependence

significantly in a rather small temperature range between 300 and 280 K, passing from one Arrhenius-like behavior at high temperatures with low activation energy to a new pronounced Arrhenius behavior with high activation energy. In contrast, real water shows a much more smoothed out transition without reaching a new Arrhenius region before homogenous nucleation sets in.

These deviations can be explained along the lines mentioned before. Compared to real water the ST2 model is known to overemphasize the local tetrahedral structure. Therefore, the tendency of the hydrogen bond network to stretch with decreasing temperature is certainly overestimated (also seen in the strong temperature dependence of the density as shown in ref 6 and Figure 1). As a consequence, the transition from the high-temperature state to the approximately four-coordinated (see Table 1) low-temperature state is completed at higher temperatures and in a much smaller temperature range than can be expected for real water. Thus, the region where the corresponding Arrhenius behavior may occur in real water might exist below the homogeneous nucleation temperature.[1]

In fact, recent estimates of the diffusion coefficient at a temperature of about 155 K indicate a nondiverging temperature dependence in deeply supercooled water.[62]

To make a closer connection between the observed temperature dependence of the dynamic properties at low temperatures and the onset of jump diffusion, we discuss Figure 11. Here, the reorientation times, τ_2, and inverse diffusion coefficients, D^{-1}, are compared with the jump diffusion times τ_0. At temperatures above 275 K, τ_0 rapidly falls below 1 ps. For shorter values of this quantity it is hard to speak of jump diffusion; rather a microstep diffusion picture seems to be appropriate there. For longer residence times, all observed dynamic properties change in parallel, revealing the dominant influence of the jump process on translation and rotation. The activation energy in this region is estimated to 115 kJ mol^{-1}, a value close to 4 times the average energy of a linear hydrogen bond.[53]

Figure 12 substantiates the physical significance of the values for τ_0, obtained from the fitting procedure described in section 4.1. It shows the center of mass mean square displacements of the water molecules in log–log scale. At each temperature, the displacement at the τ_0 value of the fitting procedure is marked. As can be seen, τ_0 corresponds to the time when the linear Einstein relation starts to be valid. For earlier times, the cage effect, discussed extensively by Sciortino et al. for SPC/E water[19,20] is evolving. Again, above 280 K no such cage effect can be detected.

5. Conclusions

We have shown that in the case of ST2 water one can clearly justify the use of the Singwi–Sjölander jump-diffusion model for the long-time behavior of the dynamic incoherent structure factor by verifying the existence of a hopping-type self-motion of the molecules in the extremely supercooled regime.[63] Additionally, we can state that the change in the underlying diffusion mechanism strongly affects the temperature dependence of translational and rotational diffusion, leading to a second region of apparent Arrhenius behavior at low temperatures. Interestingly, the transition to a hopping-type dynamics occurs in a region where the ST2 liquid transforms into a more ordered low-density form. The observed abrupt structural and thermodynamical changes are in line with the singularity-free model of Debenedetti et al.[17] But they can also be understood in the frame of the second critical point scenario worked out by Stanley and co-workers.[6,14,18]

Diffusive Motion in Deeply Supercooled Water

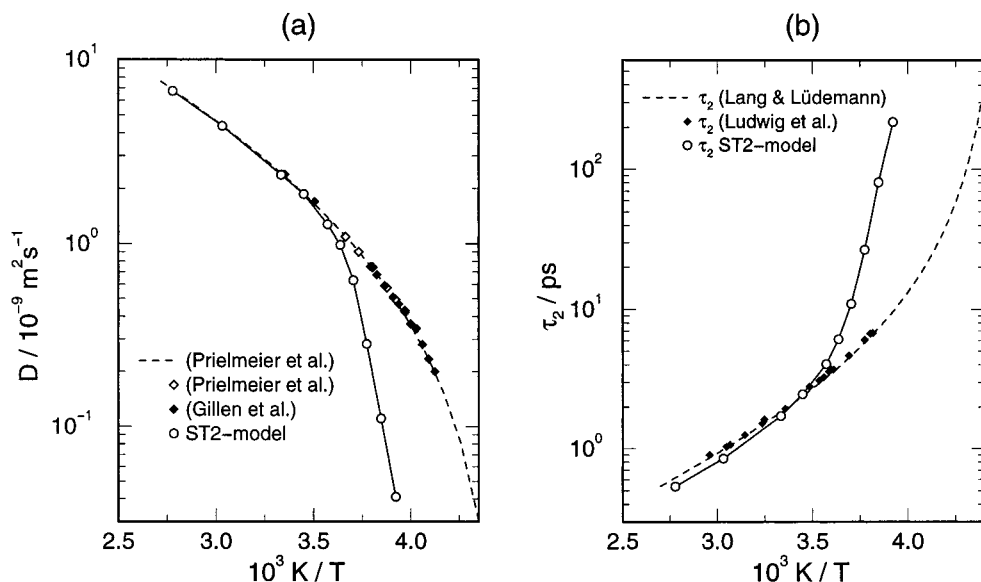*J. Phys. Chem. B, Vol. 103, No. 20, 1999* **4145**

Figure 10. Dynamical single particle properties of supercooled ST2 water. (a) Translational diffusion coefficients D for ST2 water (open circles) compared to experimental data by Prielmeier et al.[23] and Gillen et al.[57] obtained at 0.1 MPa. The dashed curve represents a fit of the experimental data to the scaling behavior $D = D_0(T/T_s - 1)^\gamma$ ($D_0 = 1.67 \times 10^{-8}$ m^2 s^{-1}, $T_s = 223$ K, $\gamma = 1.82$) according to ref 23. (b) Reorientational correlation times τ_2 (open circles) compared with experimental values from Lang and Lüdemann[59] and Ludwig et al.[60] The experimental scaling law $\tau_2 = \tau_{20}(T/T_s - 1)^{-\gamma}$ has been employed ($\gamma_{20} = 0.246$ ps, $T_s = 223$ K, $\gamma = 1.89$). To reproduce the data of Ludwig et al. τ_{20} of ref 59 was reduced by a factor of 0.72.[61]
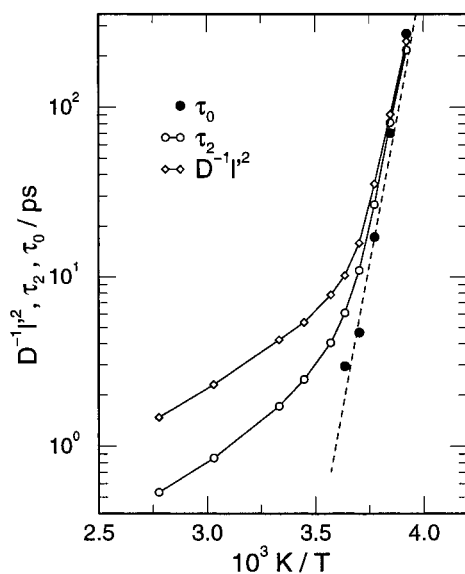

Figure 11. Comparison of the mean residence time τ_0 with the O−H vector reorientation times τ_2 and diffusion coefficients D from the simulation. The inverse diffusion coefficient D^{-1} is multiplied with the unit of length $l'^2 = 1$ Å^2. The dashed Arrhenius line corresponds to an activation energy $E_a = 115$ kJ mol^{-1}.

Considering the modified van der Waals model of Poole at al.[14] for the case of "strong" H-bonds, with decreasing temperatures our simulations are entering continuously the region of low-density supercooled water, avoiding the second critical point (see Figure 3a of[14]). The appropriateness of this phase diagram is supported by the pronounced H-bonding interaction of the ST2 model potential with a potential well depth of 28.6 kJ mol^{-1}.[26]

The high activation energy of 115 kJ mol^{-1} corresponds to a slowdown of nearly 12 orders of magnitude, when proceeding from $T = 255$ K to $T = 170$ K, τ_2 then being about 100 s. This would be a rough estimate of the ST2 glass transition temperature.[64] With the temperature shift of the ST2 phase diagram, discussed in the Introduction, this could be compared with
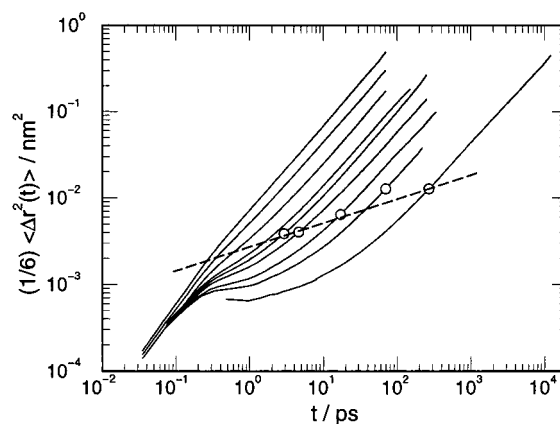

Figure 12. Log−log plot of the center of mass mean square displacement for the temperatures (from right to left) 255, 260, 265, 270, 275, 280, 300, 330, and 360 K. The circles indicate the mean square displacements at the jump times τ_0 from Table 2.

$T_g = 136$ K of real water.[64] As previously done for SPC/E water,[21] from these observations it can also be concluded for the ST2 model that there exists a continuous path connecting the liquid state and the low-density amorphous ice. In combination with the estimation that SPC/E and ST2 "bracket" the properties of real water, there is a high probability for the same situation to be true for the real substance.

In Angell's strong/fragile classification scheme[65] of glass forming liquids, a pronounced Arrhenius dependence of the dynamical properties over many orders of magnitude up to the glass transition point would suggest the low-density supercooled water to be a strong liquid.[66] On the other hand, the high activation energy of about 115 kJ mol^{-1} and the expected higher glass transition temperature would position low-density ST2 water in an intermediate range of the Angell plot.[64]

Finally, the apparent difference between the dynamics of ST2 water presented here and the SPC/E dynamics at low temperatures has to be commented on. As has been pointed out by Sciortino et al.,[19,20] a possible explanation can be found in the temperature shifts of the phase diagrams of these two model

liquids. By this, ST2 water reaches the low-density, nearly perfect tetrahedral structure at much higher temperatures than SPC/E. In this situation ST2 has enough thermal energy to escape frequently from the cage of four neighbors by jumps. In other words, the onset of jump diffusion overrides the occurrence of perfect structural arrest and thus prevents the observation of an approach to a kinetic glass transition as described by mode coupling theory[24] and as found in SPC/E water.[19,20] For real water we expect a behavior in between; the observed power law approach to the so-called Angell temperature will eventually be overcome by jump diffusion.

References and Notes

(1) Angell, C. A. In *Water: A Comprehensive Treatise*; Franks, F., Ed.; Plenum Press: New York, 1982; Vol. 7, Chapter 1.

(2) Speedy, R. J.; Angell, C. A. *J. Chem. Phys.* **1976**, *65*, 851.

(3) Speedy, R. J. *J. Phys. Chem.* **1982**, *86*, 982.

(4) Speedy, R. J. *J. Phys. Chem.* **1982**, *86*, 3002.

(5) Speedy, R. J. *J. Phys. Chem.* **1987**, *91*, 3354.

(6) Poole, P. H.; Sciortino, F.; Essmann, U.; Stanley, H. E. *Nature* **1992**, *360*, 324.

(7) Poole, P. H.; Sciortino, F.; Essmann, U.; Stanley, H. E. *Phys. Rev. E* **1993**, *48*, 3799.

(8) Poole, P. H.; Sciortino, F.; Essmann, U.; Stanley, H. E. *Phys. Rev. E* **1993**, *48*, 4605.

(9) Stanley, H. E.; Angell, C. A.; Essmann, U.; Hemmati, M.; Poole, P. H.; Sciortino, F. *Physica A* **1994**, *205*, 122.

(10) Stanley, H. E.; Cruz, L.; Harrington, S. T.; Poole, P. H.; Sastry, S.; Sciortino, F.; Starr, F. W.; Zhang, R. *Physica A* **1997**, *236*, 19.

(11) Rapaport, E. *J. Chem. Phys.* **1966**, *46*, 2891.

(12) Ponyatovsky, E. G.; Barkalov, O. I. *Mater. Sci. Rep.* **1992**, *8*, 147.

(13) Borik, S. S.; Debenedetti, P. G.; Sastry, S. *J. Phys. Chem.* **1995**, *99*, 3781.

(14) Poole, P. H.; Sciortino, F.; Grande, T.; Stanley, H. E.; Angell, C. A. *Phys. Rev. Lett.* **1994**, *73*, 1632.

(15) Stanley, H. E.; Teixeira, J. *J. Chem. Phys.* **1980**, *73*, 3404.

(16) Stanley, H. E.; Blumberg, R. L.; Geiger, A.; Mausbach, P.; Teixera, J. *J. Phys. (Paris)* **1984**, *45*, [C7]13.

(17) Rebelo, L. P. N.; Debenedetti, P. G.; Sastry, S. *J. Chem. Phys.* **1998**, *109*, 626.

(18) Mishima, O.; Stanley, H. E. *Nature* **1998**, *392*, 164.

(19) Gallo, P.; Sciortino, F.; Tartaglia, P.; Chen, S.-H. *Phys. Rev. Lett.* **1996**, *76*, 2630.

(20) Sciortino, F.; Gallo, P.; Tartaglia, P.; Chen, S.-H. *Phys. Rev. E* **1996**, *54*, 6331.

(21) Sciortino, F.; Fabbian, L.; Chen, S.-H.; Tartaglia, P. *Phys. Rev. E* **1997**, *56*, 5397.

(22) Prielmeier, F. X.; Lang, E. W.; Speedy, R. J.; Lüdemann, H. D. *Phys. Rev. Lett.* **1987**, *59*, 1128.

(23) Prielmeier, F. X.; Lang, E. W.; Speedy, R. J.; Lüdemann, H. D. *Ber. Bunsen-Ges. Phys. Chem.* **1988**, *92*, 1111.

(24) Götze, W.; Sjögren, L. *Rep. Prog. Phys.* **1992**, *55*, 241.

(25) Berendsen, H. J. C.; Grigera, J. R.; Straatsma, T. P. *J. Phys. Chem.* **1987**, *91*, 6269.

(26) Stillinger, F. H.; Rahman, A. *J. Chem. Phys.* **1974**, *60*, 1545.

(27) Harrington, S. T.; Poole, P. H.; Sciortino, F.; Stanley, H. E. *J. Chem. Phys.* **1997**, *107*, 7443.

(28) Miyagawa, H.; Hiwatari, Y.; Bernu, B.; Hansen, J. P. *J. Chem. Phys.* **1988**, *88*, 3879.

(29) von Blanckenhagen, P. *Ber. Bunsen-Ges. Phys. Chem.* **1972**, *76*, 891.

(30) Chen, S. H.; Teixera, J.; Nicklow, R. *Phys. Rev. A* **1982**, *26*, 3477.

(31) Teixera, J.; Bellissent-Funel, M. C.; Chen, S. H.; Dianoux, A. J. *Phys. Rev. A* **1985**, *31*, 1913.

(32) Bee, M. *Quasielastic Neutron Scattering*; Adam Hilger: Bristol, 1988.

(33) Chen, S. H. In *Hydrogen Bonded Liquids*; Dore, J. C. Teixera, J., Eds.; NATO ASI Series C; Kluwer Academic Publishers: Dordrecht, 1990; Vol. 293.

(34) Chen, S.-H.; Gallo, P.; Sciortino, F.; Tartaglia, P. *Phys. Rev. E* **1997**, *56*, 4231.

(35) Sjölander, A. In *Thermal Neutron Scattering*; Egelstaff, P. A., Ed.; Academic Press: London, 1965; Chapter 7.

(36) Egelstaff, P. A. *An introduction to the liquid state*; Academic Press: London, 1967.

(37) Rahman, A.; Stillinger, F. H.; *J. Chem. Phys.* **1971**, *55*, 3336.

(38) Jorgensen, W. L.; Chandrasekhar, J.; Madura, J. D.; Impey, R. W.; Klein, M. L. *J. Chem. Phys.* **1983**, *79*, 926.

(39) Baez, L. A.; Clancy, P. *J. Phys. Chem.* **1994**, *101*, 9837.

(40) Allen, M. P.; Tildesley D. J. *Computer Simulation of Liquids*; Oxford Science Publications: Oxford, 1989.

(41) Steinhauser, O. *Mol. Phys.* **1982**, *45*, 335.

(42) Berendsen, H. J. C.; Postma, J. P. M.; van Gunsteren, W. F.; DiNola, A.; Haak, J. R. *J. Chem. Phys.* **1984**, *81*, 3684.

(43) Rehtanz, A.; Poole, P. H.; Geiger, A. To be pulished.

(44) Chowdhury, M. R.; Dore, J. C.; Wenzel, J. T. *J. Non-Cryst. Sol.* **1982**, *53*, 247.

(45) Mishima, O.; Calvert, L. D.; Whalley, E. *Nature* **1984**, *310*, 393.

(46) Bellissent-Funel, M.-C.; Teixera, J.; Bosio, L. *J. Chem. Phys.* **1987**, *87*, 2231.

(47) Bellissent-Funel, M.-C.; Bosio, L. *J. Chem. Phys.* **1995**, *102*, 3727.

(48) Medvedev, N. N.; Naberukhin, Y. I. *J. Non-cryst. Solids* **1987**, *94*, 402.

(49) Bellissent-Funel, M.-C. *Europhys. Lett.* **1998**, *42*, 161.

(50) Kneller, G. R.; Geiger, A. *Mol. Phys.* **1990**, *70*, 465.

(51) van Hove, L. *Phys. Rev.* **1954**, *95*, 249.

(52) Sciortino, F.; Geiger, A.; Stanley, H. E. *Phys. Rev. Lett.* **1990**, *65*, 3452.

(53) Sciortino, F.; Geiger, A.; Stanley H. E. *Nature* **1991**, *354*, 218.

(54) Sciortino, F.; Geiger, A.; Stanley, H. E. *J. Chem. Phys.* **1992**, *96*, 3857.

(55) Abragam, A. *Principles of Nuclear Magnetism*; Clarendon Press: Oxford, 1961.

(56) Lankhorst, D.; Schriever, J.; Leyte, J. C. *Ber. Bunsen-Ges. Phys. Chem.* **1982**, *86*, 215.

(57) Gillen, K. T.; Douglas, D. C.; Hoch, M. J. R. *J. Chem. Phys.* **1972**, *57*, 5117.

(58) Lang, E. W.; Lüdemann, H. D. *Ber. Bunsen-Ges. Phys. Chem.* **1980**, *84*, 462.

(59) Lang, E. W.; Lüdemann, H. D. *Ber. Bunsen-Ges. Phys. Chem.* **1981**, *85*, 603.

(60) Ludwig, R.; Weinhold, F.; Farrar, T. C. *J. Chem. Phys.* **1995**, *103*, 6941.

(61) Concerning the dashed curve for τ_2, it should be mentioned that the original analytic expression of Lang and Lüdemann[59] has been scaled by a constant factor of 0.72. Motivation for this procedure was recent NMR measurements of Ludwig et al.,[60] who determined the quadrupole coupling constants (QCC) for *liquid* water. The liquid-phase values were found to lie between the gas-phase and ice values and showed no significant temperature dependence. The squared ratio of their liquid-phase QCC (about 253 kHz) and the value for ice (214 kHz) used in[59] is reflected by the constant factor 0.72.

(62) Smith, R. S.; Huang, C.; Kay, B. D. *J. Phys. Chem. B* **1997**, *101*, 6123.

(63) Regarding the position of the observed dynamical transition within the ST2 phase diagram, our results do not necessarily provide support for the validity of a jump-type interpretation of experimental QENS data of ambient and supercooled real water.

(64) Angell, C. A.; Poole, P. H.; Shao, J. *Il Nuovo Cimento* **1994**, *16*, 993.

(65) Angell, C. A. *J. Non-Cryst. Sol.* **1991**, *13*, 131.

(66) Angell, C. A. *J. Phys. Chem.* **1993**, *97*, 6339.